INL RPT-23-74806
Revision 0

MAGNET Scaling and Methodology

Hierarchical Two-Tiered Scaling

September | 2023

Zachary Ketrow
Graduate Student Intern, Oregon State University

Qiao Wu
Professor, Oregon State University

Ramon Yoshiura
Computational Scientist, Integrated Energy & Market Analysis

IES
Integrated Energy Systems

INL is a U.S. Department of Energy National Laboratory operated by Battelle Energy Alliance, LLC

INL RPT-23-
Revision 0

MAGNET Scaling and Methodology

Hierarchical Two-Tiered Scaling

Zachary Ketrow
Graduate Student Intern, Oregon State University
Qiao Wu
Professor, Oregon State University
Ramon Yoshiura
Computational Scientist, Integrated Energy & Market Analysis

September | 2023

Idaho National Laboratory
Integrated Energy Systems
Idaho Falls, Idaho 83415

http://www.ies.inl.gov

Prepared for the
U.S. Department of Energy
Office of Nuclear Energy
Under DOE Idaho Operations Office
Contract DE-AC07-05ID14517

Page intentionally left blank

SUMMARY

The purpose of this study was to analyze the heat transfer of the Microreactor Agile Non-nuclear Experimental Testbed (MAGNET) within the Dynamic Energy Transport and Integration Laboratory (DETAIL) and develop scaling equations and models to couple with other systems. Hierarchical two-tiered scaling (H2TS) methodologies were applied to DETAIL's MAGNET facility to scale and project data sets while conserving the observed behavior based on first principles. The MAGNET system was successfully scaled using H2TS and multiple system parameters were determined or calculated from experimental data including steady state and transient data.

Page intentionally left blank

CONTENTS

FIGURES

Page intentionally left blank

ACRONYMS

IES	Integrated Energy System
DETAIL	Dynamic Energy Transport and Integration Laboratory
DSS	Dynamical System Scaling
H2TS	Hierarchical Two-Tiered Scaling
TEDS	Thermal Energy Distribution System
SOEC	Solid-Oxide Electrolysis Cell
HTSE	High-Temperature Steam Electrolysis
INL	Idaho National Laboratory
NPP	Nuclear Power Plant
V&V	Validation and Verification
MAGNET	Microreactor Agile Non-Nuclear Experimental Testbed
MARVEL	Microreactor Applications Research Validation and Evaluation
LHS	Left-Hand Side
RHS	Right-Hand Side

Page intentionally left blank

MAGNET Scaling and Methodology

1. INTRODUCTION AND BACKGROUND

A collaborative relationship between nuclear, fossil, and renewable energy systems will ensure an internationally competitive energy pipeline that is secure, resilient, sustainable, economical, and resource efficient. The coupling produces electrical energy in magnitudes that match demand at affordable prices. Excess thermal energy can be stored for industrial processes that consume heat, such as hydrogen production, optimizing capital investments and enhancing resource usage.

Idaho National Laboratory's (INL) Integrated Energy System (IES) program seeks to demonstrate this capability by connecting subsystems in INL's Dynamic Energy Transport and Integration Laboratory (DETAIL). The DETAIL system consists of multiple subsystems that represent microreactor core thermal behavior, heat storage, electric storage, hydrogen production, power emulator, microgrid simulator, and vehicle wireless charging station and is planned to have each subsystem either physically or virtually connected.

The goal is to virtually connect DETAIL subsystems to other INL internal facilities, external laboratories, and commercial entities retrieving input signals to benchmark the IES from lab scale to pilot scale. With online data transfer from other systems, DETAIL will simultaneously emulate the IES framework as if actual utilities were connected and readjusting power production to accommodate the dynamic response of consumer demand during normal conditions and unanticipated events.

2. MAGNET FACILITY

Microreactors, or small, transportable reactors with a capacity of < 20 MWT, provide heat and power for myriad applications in remote areas, military installations, emergency operations, humanitarian missions and disaster relief zones. These small, transportable reactor designs, while offering many advantages, are largely untested and unproven. System and component testing is needed to demonstrate to regulators that these designs are safe and to convince customers that the systems are robust, reliable, and efficient.

2.1. MAGNET Overview

The microreactor agile non-nuclear experimental test bed (MAGNET), shown in Figure 2.1, in the Energy Systems Laboratory (ESL) High Bay, D100, provides the capability to develop, demonstrate, and validate microreactor components and systems. MAGNET supports technology maturation to reduce uncertainty and risk relative to the operation and deployment of this unique class of systems. Stakeholders for MAGNET include microreactor developers, energy users, and regulators. Within MAGNET, systems and components can be safely tested, providing valuable information on operating modes, failure modes, and thresholds. Since there are various types of microreactors being proposed, which can be classified according to their core cooling method (e.g., heat pipe, gas-cooled (pebble bed or prismatic), molten salt, or light-water), the goal of this study focuses on the initial set of tests to be performed in MAGNET. These initial tests assert the feasibility and performance of heat pipe-cooled reactors, since this concept is unique to very small nuclear reactors. However, MAGNET has been designed to accommodate other designs in addition to heat pipe-cooled reactors. To increase the technological maturity of microreactors, MAGNET is designed to:

- Provide a general-purpose test bed for performance evaluation of microreactor design concepts (heat pipe, gas-cooled, other).
- Provide detailed reactor core and heat removal section thermal-hydraulic performance data for prototypical geometries and operating conditions.
- Enhance the readiness of novel reactor components such as heat pipes.

- Provide test article and flow loop temperature-time histories during reactor startup, shutdown, steady-state, and off-normal operations.
- Provide displacement and temperature field data for potential design performance verification and accompanying analytical model validation.
- Evaluate the interface between simulated reactor components and the primary heat removal heat exchanger for both geometric compatibility, functionality, and heat transfer capability.
- Test the interface of the reactor heat removal heat exchanger to auxiliary systems, such as power conversion systems for energy production or process heat applications.
- Evaluate concepts for passive decay-heat removal.
- Measure the effects of non-uniform heating profiles.
- Determine the effects of heat pipe or flow channel (both single and cascade) failures.
- Identify and develop advanced sensors and power conversion equipment including instrumentation for autonomous operation and for in-operando data collection and monitoring.
- Assess structural integrity of the core block, i.e., thermal stress, strain, aging/fatigue, creep, deformation.
- Study the effects of cyclic loading on materials and components.
- Demonstrate the applicability of advanced manufacturing techniques, such as additive manufacturing and diffusion bonding, for nuclear reactor applications.
- Enhance readiness of the public stakeholders—particularly Department of Energy (DOE) laboratories and the United States Nuclear Regulatory Commission (NRC)—to design, operate, and test high-temperature reactor components.

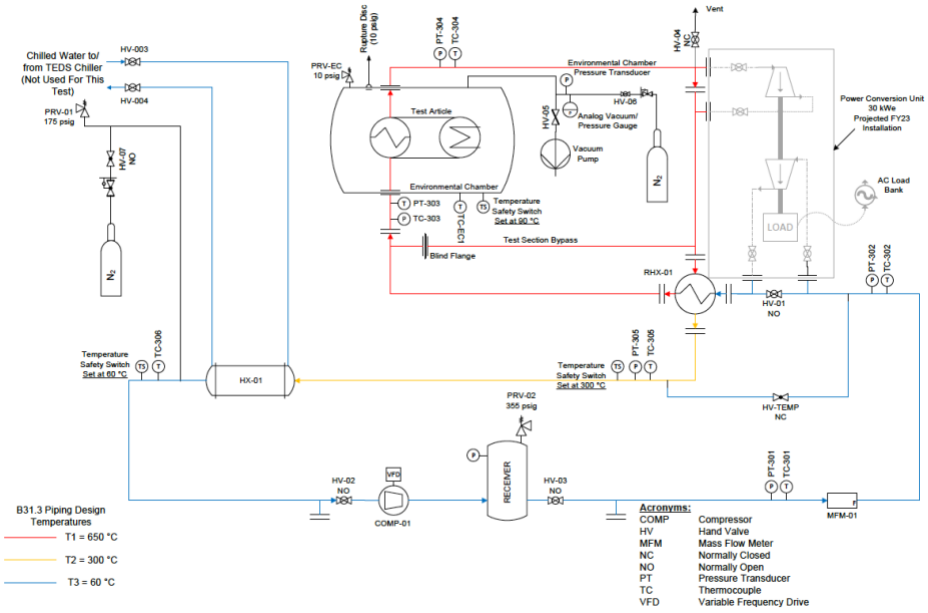

Figure 2.1 MAGNET process-flow diagram [1].

2.2. MAGNET for Heat Pipe Testing

Heat Pipe Testing System

For the single heat pipe test, since there is only one heat pipe with a total heat removal rating of 1 kW, the heater heat fluxes are limited by the heat transfer rating of the heat pipe. This limitation results in the use of significantly lower heat fluxes than the full prototypical core design values. Heat pipe operating temperatures are limited to 750°C. The vapor pressure of sodium at 750°C is approximately 25% of atmospheric pressure; therefore, over-pressurization failure of the heat pipe is not a realistic safety consideration, which is to say, the heat pipe operates at a vacuum at temperatures of 750°C and below.

Test articles have been subjected to a maximum of 750°C. They were housed inside the environmental chamber and accessible during operation. Piping insulation maintains surface temperatures less than120°F. During operation, insulation surface temperatures are surveyed to determine if there are areas exceeding this temperature. Pre-operational briefings and barriers with appropriate signage can mitigate risk for surface temperatures exceeding 120°F.

Heat pipes with a sodium working fluid and a supplier-specific wick structure are fabricated from stainless-steel tubing. The total quantity of sodium in each heat pipe is less than 100 g (approximately 60 – 80 g [1]). After filling, the heat pipes are seal welded under a vacuum. The heat pipes are passive, fully sealed devices that will be operated within their design limits. This work does not involve any direct handling of sodium. As noted previously, pressure inside the heat pipes is sub-atmospheric even at the highest operating temperature, so any failure of the heat pipe would not involve a pressurized release of material.

The test article is a seven-hole, single heat pipe-cooled, hexagonal "core block" with the cross-sectional geometry shown in Figure 2.2. The core block material is stainless-steel 316 L and is 1 m in length. The outer ring of six holes in the core block will be fitted with electric resistance cartridge heaters. Heat from the condenser end of the heat pipe will be removed by N_2 gas flow through an annular space surrounding the heat pipe (Figure 2.3). A small, coiled, tube-in-tube, counterflow, sentry heat exchanger is installed inside the environmental chamber and is used for heat recovery during the initial, low-flow tests in MAGNET. When experimentation shifts to full-sized test articles, this temporary, tube-in-tube HX is removed. For the single heat pipe test article, NFPA-484 is not applicable based on the quantity of sodium in use.

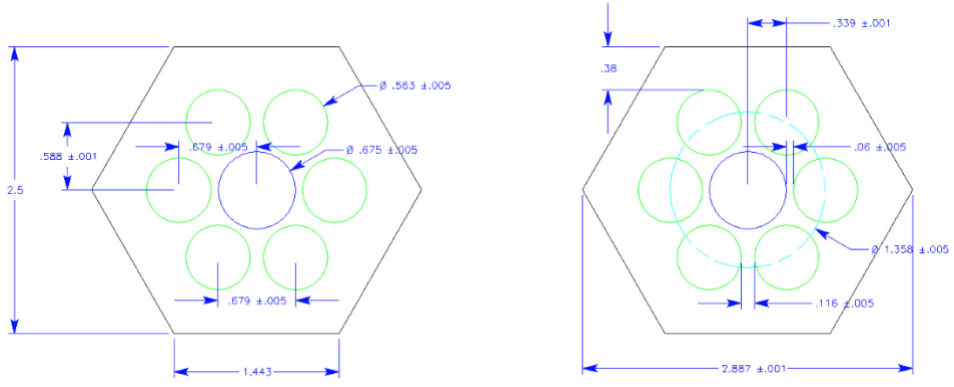

Figure 2.2. Cross-Sectional Drawing of Core Block for Single Heat Pipe Experiment [1].

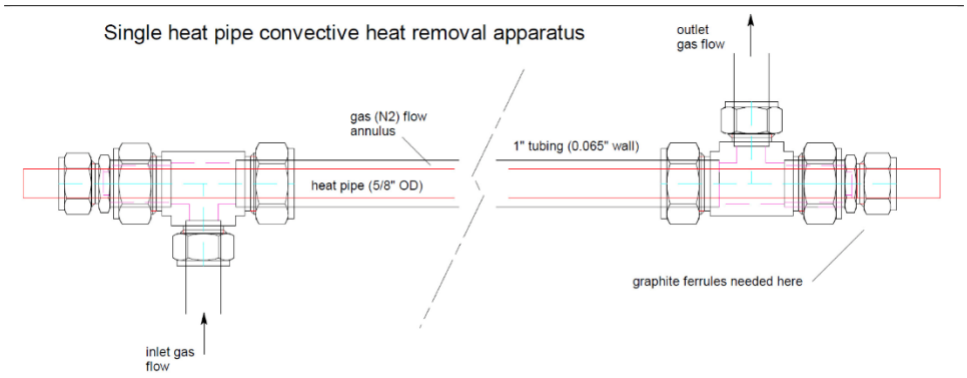

Figure 2.3 Plan-view of diagram of single heat pipe gas convection heat removal apparatus [1].

The hex block sat on a two one-inch, square, steel tubes (shown in Figure 2.4 for an image of the test article in the environmental chamber). The heat pipe was supported by a v block and 1/8" aramid insulation. The calorimeter was supported by a v block with no insulation.

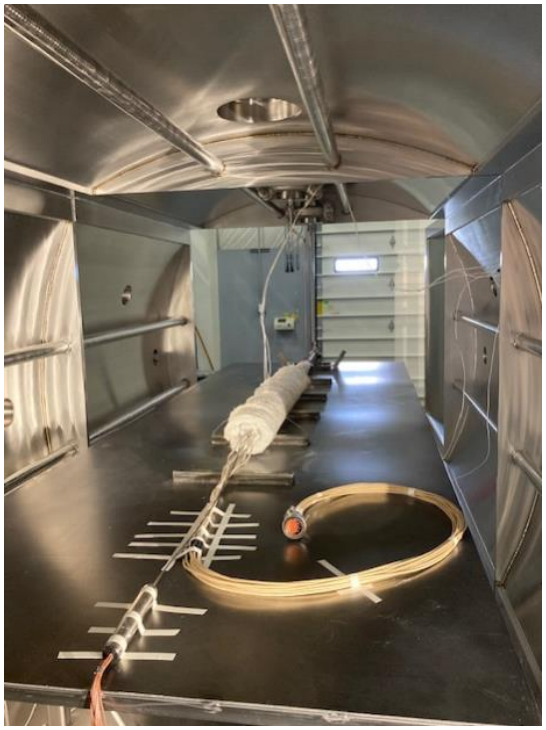

Figure 2.4 Image of the test article in the environmental chamber [1].

The objectives of the single heat pipe testing in MAGNET include:

- Demonstrate the operation of MAGNET while operating a single heat pipe microreactor mockup through a range of operating parameters.
- Observe heat pipe start up and transient operation with convective gas cooling by recording time-dependent operating data of the heaters, the heat pipe, and the core block. These data establish a knowledge basis and operating experience for future testing of multiple heat pipes.

Quantify the effectiveness of thermal coupling methods between the heat pipe and cartridge heater outer surfaces and the core block by measuring heater, heat pipe, and core block temperatures over a range of operating temperatures. The parameters are provided below.

Heaters, Watlow FIREROD cartridge heaters:

- 36” in length
- 3000 W (rated at 240V/1PH)
- 53 W/in^2 (rated)

Heater Controllers:

- Protherm heater control panel—208V, 1PH, 80A
- Three over temperature limit controllers in series—all open a main solenoid on hot and neutral 208 V supply
- PID temperature control with two zones (three heaters in each zone)
- Ground fault interrupt.

Data Acquisition:

- National Instruments SCXI data acquisition system.

High-temperature heat pipes with advanced cooling technologies:

- Pipe material: SS 316
- Geometry: smooth-wall tube, screen wick, thermo-well
- Length: 2 m, Diameter: 0.625-inch
- Working fluid: sodium, with non-condensable inert gas
- Wick: screen, 40 mesh 304 SS, 250 μm wire diameter
- Operating temperature, ~740°C
- Heat removal rating: 1000 W.

Heat Pipe Testing Results

INL staff completed the single heat pipe test campaign in MAGNET on March 30, 2022, in the INL Energy Systems Laboratory (ESL). MAGNET and single heat pipe test articles were run through a series of excursions to demonstrate operation of MAGNET including its ability to control test article temperature, control gas cooling flow rate, acquire and record instrumentation outputs, and allow integration of a digital twin (DT).

MAGNET through the following test plan:

1. Start compressor (CMP-01) at 10 Hz and monitor flow rate at mass flow meter MFM-01until it is stable at approximately 45 kg/h. Check differential pressure on local gauges at compressor and record in the electronic laboratory notebook (ELN).

2. Raise CMP-01 frequency to 15 Hz and monitor flow rate at MFM-01 until it is stable at approximately 140 kg/h. Check differential pressure on local gauges at compressor and record in the ELN.
3. Raise CMP-01 frequency to 20 Hz and monitor flow rate at MFM-01 until it is stable at approximately 200 kg/h. Check differential pressure on local gauges at compressor and record in the ELN. If differential pressure approaches 45 psi, skip remaining frequency ramps and go on to step F.
4. Raise CMP-01 frequency to 25 Hz and monitor flow rate at MFM-01 until it is stable at approximately 240 kg/h. Check differential pressure on local gauges at compressor and record in the ELN. If differential pressure approaches 45 psi, skip remaining frequency ramps and go on to step.
5. Raise CMP-01 frequency to 30 Hz and monitor flow rate at MFM-01 until it is stable at approximately 280 kg/h. Check differential pressure on local gauges at compressor and record in the ELN.
6. Set heater controller to 500°C with a ramp rate of 500°C per hour.

   HOLD POINT: 500°C is the temperature at which the heat pipe should become active (lower end of temperature range for sodium heat pipes). Monitor test article temperature until its temperature increase is less than 5°C per hour.

   NOTE: The heat pipe, when active, will be isothermal (meaning there will be very little temperature gradient along its length). The first indication of a heat pipe failure will be an increase in the temperature gradient beyond 100°C. Past 500°C, monitor the heat pipe temperatures. Stop all heaters and stop compressor for any rise in axial temperature gradient beyond 100°C.

   NOTE: Monitor environmental chamber temperature and stop heaters if temperature exceeds 90°C.
7. Raise heater controller set point to 600°C and monitor test article temperatures until they rise less than 5°C per hour.
8. Lower heater temperature set point to 500°C.
9. Begin DT integration by turning on LabVIEW HMI feature that allows reading of DT output files and application of requested DT changes such as temperature set point changes.
10. Raise heater controller set point to 550°C and monitor core block and heat pipe temperatures from DT. Verify LabVIEW reads DT output and adjusts temperature set point back to 500°C.
11. Verify heater controller set point at 500°C and wait until test article temperatures change less than 5°C per hour.
12. Lower heater controller set point to 450°C and monitor core block and heat pipe temperatures from DT. Verify LabVIEW reads DT output and adjusts temperature set point back to 500°C.
13. Raise heater controller set point to 550°C with ramp rate of 500°C per hour.
14. Raise heater controller set point to 600°C with ramp rate of 90°C per hour.
15. If CMP-01 dP is less than 30 psi, raise CMP-01 frequency to 40 Hz and monitor flow rate at MFM-01 until it is stable at approximately 370 kg/h. Observe heater and heat pipe temperatures. If dP is greater than 30 psi, skip to Step 18.
16. If CMP-01 dP is less than 30 psi, raise CMP-01 frequency to 50 Hz and monitor flow rate at MFM-01 until it is stable at approximately 540 kg/h. If dP is greater than 30 psi, skip to Step 18.

17. If CMP-01 dP is less than 30 psi, raise CMP-01 frequency to 60 Hz and monitor flow rate at MFM-01 until it is stable at approximately 1000 kg/h.
18. Stop heaters.
19. Lower CMP-01 frequency to 30 Hz and run for 30 minutes.
20. Stop CMP-01 and shut down remainder of system.

The test results are summarized in Figure 2.5 and Figure 2.6. Figure 2.5 shows plots of heater set point and heat pipe temperatures as functions of time. Figure 2.6 shows a plot of mass flow rate as a function of time. Actual flow rates measured were lower than anticipated due to the small cross-sectional flow area of the gas gap calorimeter. Heater controls worked well in both steady power and temperature control modes. Since the heat pipe was not in physical contact with either the core block or the calorimeter, no significant heat transfer to the gas coolant loop of MAGNET was demonstrated.

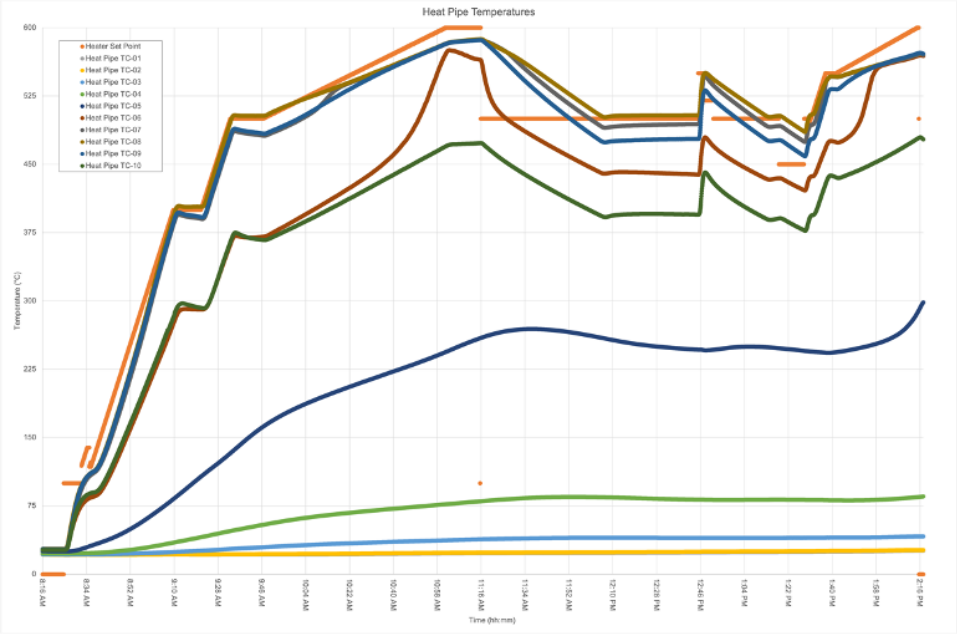

Figure 2.5 Heat pipe temperature transient. Through TC-01 and TC-10, are the axial heat pipe temperatures 5 inches apart where TC-01is in the heater section and TC-10 is in the condenser section.

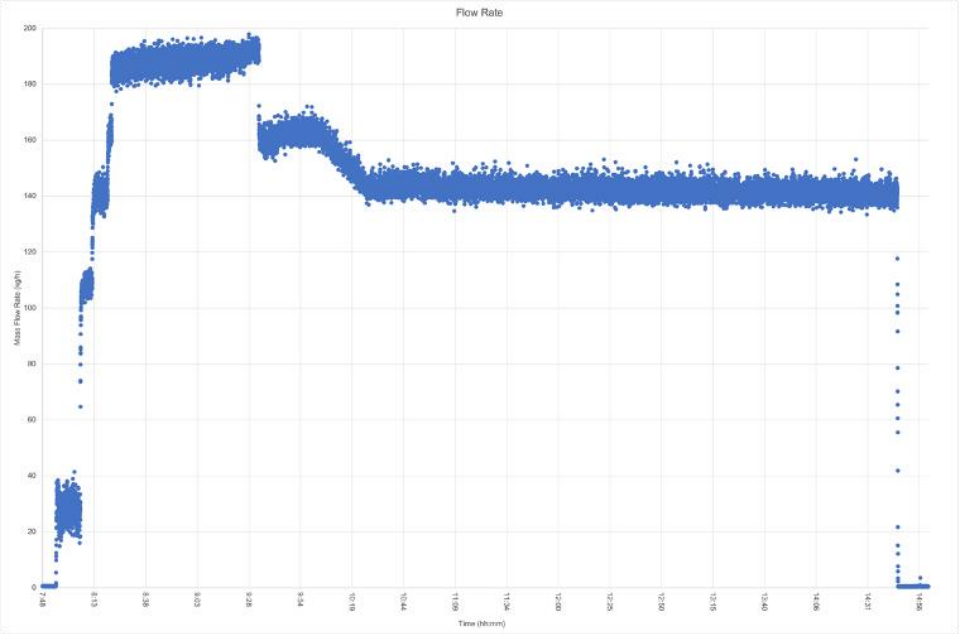

Figure 2.6 Heat pipe cooling mass flow rate transient.

3. HIERARCHICAL TWO-TIERED SCALING THEORY

The hierarchical two-tiered scaling (H2TS) theory consists of four fundamental domains: subdivision of interacting systems, identification of scaling level, system scaling analysis, and process system scaling analysis [2]. The subdivision and scaling identification is accomplished by conducting a Phenomena Identification and Ranking Table (PIRT) activity to discern the existing subsystems, modules, constituents, and phases. Depending on the weighting of each component and developed equations, the scaling emphasis on either system scaling analysis (also called top-down scaling) or process scaling analysis (also called bottom-up scaling) may differ from one project to another. In some cases, a top-down scaling reveals important processes that may need to be addressed in the bottom-up scaling.
To express each H2TS task, the conserved quantity within a control volume equation format will be used as the main starting point for describing H2TS terminologies:

$$\frac{dV_l\psi_l}{dt} = S_l + \sum_{x=1}^{m} j_{l,x}A_{l,x} + \sum_{x=1}^{m} \psi_{l,x}\left(v_{l,x} - v_{s,l,x}\right)A_{l,x} \qquad 1$$

Where volumetric, surface, and quantity transport are provided for each constituent l. V_l is the control volume, ψ_l is the conserved quantity per volume, S_l is the volumetric source or sink, j_l is the quantity flux, A_l is the sectional area, v_l is the fluid velocity, and $v_{s,l}$ control volume surface velocity. For simplicity, the fluid velocity difference will be expressed as Δv. Terms holding units are replaced with the following dimensionless form:

$$V_l^+ = \frac{V_l}{V_{l,0}}, \quad \psi^+ = \frac{\psi_l}{\psi_{l,0}}, \quad S_l^+ = \frac{S_l}{S_{l,0}}, \quad j_{l,x}^+ = \frac{j_{l,x}}{j_{l,x,0}}, \quad A_{l,x}^+ = \frac{A_{l,x}}{A_{l,x,0}}, \quad \psi_{l,x}^+ = \frac{\psi_{l,x}}{\psi_{l,x,0}},$$
$$\Delta v_{l,x}^+ = \frac{\Delta v_{l,x}}{\Delta v_{l,x,0}} \qquad 2$$

Replacing terms in dimensionless form into the balance equation, the dimensionless balance equation is:

$$V_{l,0}\psi_{l,0}\frac{dV_l^+\psi_l^+}{dt} = S_{l,0}S_l^+ + \sum_{x=1}^{m} j_{l,x,0}A_{l,x,0}j_{l,x}^+A_{l,x}^+ + \sum_{x=1}^{m}\psi_{l,x}\Delta v_{l,x,0}A_{l,x,0}\psi_{l,x}^+\Delta v_{l,x}^+A_{l,x}^+ \quad 3$$

The first task in H2TS is to derive the residence time. This specialized temporal quantity is used to determine how long a certain system or process transient prevails. For steady state analysis, the residence time is still used to determine system similarity or calculate the full-time duration of the scaled phenomenon of interest:

Residence Time:

$$\tau_{RS} = \frac{V_{l,0}\psi_{l,0}}{S_{l,0}} \quad 4$$

In this case, the residence time is defined to be division between the reference conserved quantity and reference source or sink. The unit is the inverse of the per time quantity. To extract meaningful information that is utilized to determine the components affecting the conversed quantity, the characteristic time ratio for each component of change is derived in dimensionless form and describes the relative evolution of the component transient. Considering the residence time equation, the characteristic time ratios can be determined from the dimensionless balance equation:

$$\tau_{RS}\frac{dV_l^+\psi_l^+}{dt} = S_l^+ + \sum_{x=1}^{m}\frac{j_{l,x,0}A_{l,x,0}}{S_{l,0}}j_{l,x}^+A_{l,x}^+ + \sum_{x=1}^{m}\frac{\psi_{l,x,0}\Delta v_{l,x,0}A_{l,x,0}}{S_{l,0}}\psi_{l,x}^+\Delta v_{l,x}^+A_{l,x}^+ \quad 5$$

Each component coefficient about reference values is dimensionless and can be shown as the following:

$$\Pi_1 = \frac{j_{l,x,0}A_{l,x,0}}{S_{l,0}}, \qquad \Pi_2 = \frac{\psi_{l,x,0}\Delta v_{l,x,0}A_{l,x,0}}{S_{l,0}} \quad 6$$

In full form, the dimensionless balance equation is represented as:

$$\tau_{RS}\frac{dV_l^+\psi_l^+}{dt} = S_l^+ + \sum_{x=1}^{m}\Pi_1 j_{l,x}^+A_{l,x}^+ + \sum_{x=1}^{m}\Pi_2\psi_{l,x}^+\Delta v_{l,x}^+A_{l,x}^+ \quad 7$$

Depending on the quantity of each characteristic time ratio, the following are behaviors determined by the reference value combinations: (1) if smaller than 1, only a small amount of the conserved quantity is transported relative to the generated or destroyed amount, and (2) if equal to 1 or larger, relatively significant amounts of the conserved quantity are transported. If the denominator of characteristic time ratios $\Pi_1$and Π_2 included $\psi_{l,0}$, then relative target is the conserved quantity reference value. Decisions upon selecting which combinations to derive residence time and characteristic time ratio can affect how users interpret the relations of conserved quantity and its components of change.

The scaling aspect of H2TS is to determine the model system geometry and environment conditions based on system similarity. This includes matching characteristic time ratio values that have been identified in the PIRT process.

$$\Pi_P = \Pi_M \quad 8$$

An example can be shown for the quantity flux characteristic time ratio by considering the protype and model reference values:

$$\Pi_P = \left.\frac{j_{l,x,0}A_{l,x,0}}{S_{l,0}}\right|_P = \left.\frac{j_{l,x,0}A_{l,x,0}}{S_{l,0}}\right|_M = \Pi_M \quad 9$$

Depending on the reference value flexibility, some parameters are possibly unchangeable and may restrict the model design. In the case where model quantity flux is forced to be equal to prototype values and the model conserved quantity generation or the sink is half, the reference surface area must be half as well:

$$j_{l,x,0}\big|_M = j_{l,x,0}\big|_P, S_{l,0}\big|_M = \frac{S_{l,0}\big|_P}{2} \rightarrow A_{l,x,0}\big|_M = \frac{A_{l,x,0}\big|_P}{2} \quad 10$$

Although it would be ideal to match all characteristic time ratios, it is said to be impossible, and negligence of discarded terms are sources of scaling distortion [2].

4. MAGNET ENERGY BALANCE

The MAGNET heat pipe testing involves three parts of energy balance equations, including the control volumes of the heating block, the heat pipe and the cooling gas flow system. Two approaches are considered here for one-dimensional energy balance and a lumped energy balance.

4.1. One-Dimensional Energy Balance Equations

4.1.1. Solid Heat Block Energy Balance and Scaling

Starting with transient conduction for the solid, the solid density (ρ_s), solid specific heat capacity (C_s), solid volume occupied (ΔV_s), solid temperature (T_s), heat in ($\dot{Q}_{in}$) and heat out ($\dot{Q}_{out}$) are defined.

$$\left(\rho_s C_s \Delta V_s \frac{dT_s}{dt}\right) = \dot{Q}_{in} - \dot{Q}_{out} \quad 11$$

Expanding the $\dot{Q}_{in}$ and $\dot{Q}_{out}$ terms, the heat conduction in ($\dot{Q}_{in,cond}$), heat generation ($\dot{Q}_{in,generation}$), heat conduction out ($\dot{Q}_{out,cond}$), heat convection out ($\dot{Q}_{out,conv}$), heat radiation out ($\dot{Q}_{out,radiation}$), and boundary heat out ($\dot{Q}_{out,boundary}$) are also defined:

$$= \dot{Q}_{in,cond} + \dot{Q}_{in,generation} - \left[\dot{Q}_{out,cond} + \dot{Q}_{out,conv} + \dot{Q}_{out,radiation} + \dot{Q}_{out,boundary}\right] \quad 12$$

The heat injected into the system through conduction is a function of effective heat transfer surface area (A_s) and heat flux along the axial direction (q_s''):

$$\dot{Q}_{in,cond} = A_s q_s''(z) \quad 13$$

Heat generation from the electrical cartridge rod heaters considers the effective solid thermal energy generation ($\dot{Q}_s$), solid length (L), and applied axial direction (Δz):

$$\dot{Q}_{in,generation} = \frac{\dot{Q}_s}{L}\Delta z$$

14

The heat conduction-out term through the block in the z direction is then displaced from the heat conduction in:

$$\dot{Q}_{out,cond} = A_s q_s''(z + \Delta z)$$

15

To determine the heat removal term from the block to the heat pipe, the pipe diameter (D), the convective heat transfer coefficient ($h_{s,hp}$), and temperature difference between T_s and heat pipe temperature (T_{hp}) is used:

$$\dot{Q}_{out,conv} = \frac{(\pi D)\Delta z}{A_{s,hp}} h_{s,hp}\big(T_s(z) - T_{hp}(z)\big)$$

16

For radiative heat removal from the block to chamber, the emissivity (ε), Stefan-Boltzmann constant (σ), outer solid area (A), solid outer surface temperature (T_{sur}) and ambient temperature (T_{amb}) are defined:

$$\dot{Q}_{out,rad\rightarrow env} = \varepsilon A\sigma\big(T_{sur}^4 - T_{amb}^4\big)$$

17

Since the block is insulated in the test, the radiative heat transfer to ambient can be negligible. Therefore, the solid energy balance for the block material is given by:

$$\left(\rho_s C_s A_s \frac{dT_s}{dt}\right)\Delta z = A_s\big(q_s''((z + \Delta z) - q_s''((z)\big) + \frac{\dot{Q}_s}{L}\Delta z - [(\pi D)\Delta z]\, h_{s,hp}\left(T_s(z) - T_{hp}(z)\right)$$

18

To simplify Eq. 18 divide through by Δz and multiply L to the equation:

$$\left(\rho_s C_s A_s L \frac{dT_s}{dt}\right) = -\frac{A_s L d q_s''}{dz} + \dot{Q}_s - [L(\pi D)]\, h_{s,hp}\left(T_s(z) - T_{hp}(z)\right)$$

19

Dividing Eq. 19 through by the maximum solid thermal energy ($\dot{Q}_{s,max}$) will normalize the entire equation:

$$\frac{\left(\rho_s C_s A_s L \frac{dT_s}{dt}\right)}{\dot{Q}_{s,max}} = -\frac{\frac{A_s L dq_s''}{dz}}{\dot{Q}_{s,max}} + \frac{\dot{Q}_s}{\dot{Q}_{s,max}} - \frac{[L(\pi D)]\, h_{s,hp}\left(T_s(z) - T_{hp}(z)\right)}{\dot{Q}_{s,max}}$$

20

Where the normalized effective solid thermal energy generation ($\dot{Q}_s^+$) is the following:

$$\dot{Q}_s^+ = \frac{\dot{Q}_s}{\dot{Q}_{s,max}}$$

21

Defining the maximum temperature difference (ΔT_{max}) between the maximum surface temperature of the block ($T_{s,max}$) and the minimum temperature of the heat pipe ($T_{hp,min}$) will help to normalize solid temperature:

$$\Delta T_{max} = \left(T_{s,max} - T_{hp,min}\right)$$

22

Thus, the normalized block temperature term (T_s^+) is:

$$T_s^+(z) = \frac{T_s(z)}{\Delta T_{max}}$$

23

Similarly, for the heat pipe, the normalized heat pipe temperature (T_{hp}^+) can be determined:

$$T_{hp}^+(z) = \frac{T_{hp}(z)}{\Delta T_{max}}$$

24

The solid convection Π group is then about the balance between the maximum convection heat transfer and maximum solid thermal energy:

$$\Pi_{hp,conv} = \frac{L[(\pi D)]\, h_{s,hp} \Delta T_{max}}{\dot{Q}_{s,max}}$$

25

The normalized z position (z^+) is given by the length of the block:

$$z^+ = \frac{z}{L}$$

26

For the heat conduction Π group, the normalization process involves reorganizing the coupled conduction terms and maximum solid thermal energy:

$$\frac{\frac{LA_s dq_s''}{dz}}{\dot{Q}_{s,max}} = -\frac{kA_s \Delta T_{max}}{\dot{Q}_{s,max} L^2} \frac{\partial^2 T_s(z)^+}{\partial^2 z^+}$$

27

Thus, the solid conduction Π group is:

$$\Pi_{s,cond} = \frac{kA_s \Delta T_{max}}{\dot{Q}_{s,max} L}$$

28

Where the solid conduction Π group is then about the balance between the maximum conduction heat transfer and maximum solid thermal energy. This can also be expressed as the following:

$$\frac{\frac{LA_s dq_s''}{dz}}{\dot{Q}_{s,max}} = -\frac{\Pi_{s,cond}}{L} \frac{\partial^2 T_s(z)^+}{\partial^2 z^+}$$

29

Substituting the normalized terms from Eqs. 20, 25, and 28, the balance of the Π groups is:

$$\frac{L\left(\rho_s C_s A_s \frac{dT_s}{dt}\right)}{\dot{Q}_{s,max}} = -\Pi_{s,cond} \frac{\partial^2 {T_s}^+}{\partial^2 z^+} + \dot{Q}_s^+ - \Pi_{hp}\left(T_s^+ - T_{hp}^+\right)$$

30

Reorganizing the terms, the residence time (τ) can be derived as the following:

$$\tau = \frac{L(\rho_s C_s A_s \Delta T_{max})}{\dot{Q}_{s,max}}$$

31

The normalized time (t^+) is expressed by dividing the time (t) by the residence time. Back into the original equation, the residence time is strategically placed to normalize time.

$$t^+ = \frac{t}{\tau}$$

$$\tau \frac{dT_s^+}{dt} = -\Pi_{s,cond} \frac{\partial^2 {T_s}^+}{\partial^2 z^+} + \dot{Q}_s^+ - \Pi_{hp}\left(T_s^+ - T_{hp}^+\right)$$

32

Rearranging Eq. 32:

$$\frac{dT_s^+}{dt^+} = -\Pi_{s,cond} \frac{\partial^2 {T_s}^+}{\partial^2 z^+} + \dot{Q}_s^+ - \Pi_{hp}\left(T_s^+ - T_{hp}^+\right)$$

33

We finally get the fully normalized solid energy balance equation for the block material:

$$\frac{dT_s^+}{dt^+} = -\Pi_{s,cond} \frac{\partial^2 {T_s}^+}{\partial^2 z^+} + \dot{Q}_s^+ - \Pi_{hp,conv}\left(T_s^+ - T_{hp}^+\right)$$

34

The left-hand side (LHS) term represents the dimensionless energy change rate within the block. The first term on the right-hand side (RHS) represents the axial heat conduction along the block in the z-direction, the second term the heat generation rate from heater rods, the third term the heat transfer rate from the block to the heat pipe, and the final term the radiative heat loss from the block surface to ambient. Since the block surface is insulated shown in Figure 2.4, the radiative heat loss could be very small and therefore negligible.

Since the block is insulated, the boundary conditions for both sides of the block and their dimensionless forms should be:

$$\frac{\partial T_s(z)}{\partial z} = 0, for\ z = 0\ \&\ L$$

35

and

$$\frac{\partial T_s(z)^+}{\partial z^+} = 0, for\ z^+ = 0\ \&\ 1$$

36

4.1.2. Heat Pipe Energy Balance and Scaling

The heat pipe energy balance is identical to the solid heat transfer equation introduced in Eq. 18 as the it is just the reversed heat transfer in reference to the heat pipe without heat generation terms. The LHS is the heat pipe heat storage and the RHS represents the convective and conductive heat transfer modes:

$$\Delta z\left(\rho_{hp}C_{hp}A_{hp}\right)\frac{\partial T_{hp}}{\partial t} = \left(\pi \mathrm{D}_{hp}\Delta z\right)h_{s,hp}\left(T_s(z) - T_{hp}(z)\right) + A_{s,hp}\left(q''_{hp}(z+\Delta z) - q''_{hp}(z)\right)$$

37

Where ρ_{hp} is the heat pipe fluid density, C_{hp} is the heat pipe fluid specific heat capacity, A_{hp} is the heat pipe inner area, and q''_{hp} is the heat pipe heat flux. The heat flux is defined by the axial temperature distribution and conductive heat transfer coefficient (k). The boundary condition conductive heat transfer ($\dot{Q}_c$) is described using the mid-way heat flux and the corresponding effective solid heat transfer area:

$$q''_{hp}\left(z = \frac{L}{2}\right)A_{s,hp} = \dot{Q}_c$$

38

$$q''_{hp} = -k\frac{dT}{dz}$$

39

Apply the conductive heat transfer terms into Eq. 39:

$$\left(\rho_{hp}C_{hp}A_{hp}\right)\frac{\partial T_{hp}}{\partial t} = \left(\pi \mathrm{D}_{hp}\right)h_{s,hp}\left(T_s(z) - T_{hp}(z)\right) - A_{s,hp}k\frac{dT}{dz}$$

40

Divide through by dz to remove axial dependencies:

$$\rho_{hp}C_{hp}A_{hp}\frac{\partial T_{hp}}{\partial t} = (\pi D)h_{s,hp}\left(T_s(z) - T_{hp}(z)\right) - A_{s,hp}k\frac{d^2T}{dz^2}$$

41

Divide through by $\dot{Q}_{s,max}$ to normalize terms:

$$\frac{\rho_{hp}C_{hp}A_{hp}\frac{\partial T_{hp}}{\partial t}}{\dot{Q}_{s,max}} = \frac{(\pi D)h_{s,hp}\left(T_s(z) - T_{hp}(z)\right)}{\dot{Q}_{s,max}} - \frac{A_{s,hp}k\frac{d^2T}{dz^2}}{\dot{Q}_{s,max}}$$

42

Concentrating on the normalized heat pipe conduction term, the heat pipe conduction Π group can be derived:

$$\frac{A_{s,hp}k\frac{d^2T}{dz^2}}{\dot{Q}_{s,max}} = -\frac{kA_{hp}}{\dot{Q}_{s,max}}\frac{\partial^2 T_{hp}(z)}{\partial^2 z}$$

43

$$\frac{A_{s,hp}k\frac{d^2T}{dz^2}}{\dot{Q}_{s,max}} = -\frac{kA_{hp}\Delta T_{max}}{\dot{Q}_{s,max}L^2}\frac{\partial^2 {T_{hp}}^+}{\partial^2 z^+}$$

44

Thus, the heat pipe conduction Π group is about the balance of maximum heat pipe conductive heat transfer and maximum solid thermal energy.

$$\Pi_{hp,cond} = \frac{kA_{hp}\Delta T_{max}}{\dot{Q}_{s,max}L}$$

45

Again, this can also be expressed as the Eq. 29:

$$\frac{A_{s,hp}k\frac{d^2T}{dz^2}}{\dot{Q}_{s,max}L} = -\Pi_{hp,cond}\frac{\partial^2 {T_{hp}}^+}{\partial^2 z^+}$$

46

Plugging in the known terms from the conductive Π group, the intermediate form of the heat pipe energy balance (Eq. 42) is:

$$\frac{L\left(\rho_{hp}C_{hp}A_{hp}\right)\Delta T_{max}}{\dot{Q}_{s,max}}\frac{\partial {T_{hp}}^+}{\partial t} = \frac{(\pi D)h_{s,hp}\Delta T_{max}\left({T_s}^+ - {T_{hp}}^+\right)}{\dot{Q}_{s,max}} - \Pi_{hp,cond}\frac{\partial^2 {T_{hp}}^+}{\partial^2 z^+}$$

47

Defining the maximum temperature difference between the surface of the block and the minimum of the heat pipe as in Eq. 22 will allow to normalize temperature terms:

$$\Delta T_{max} = \left(T_{s,max} - T_{hp,min}\right)$$

48

Using Eq. 48, the normalized solid surface temperature (T_s^+) term is:

$$T_s^+(z) = \frac{T_s}{\Delta T_{max}}$$

49

Similarly, the normalized heat pipe temperature (T_{hp}^+) term is:

$$T_{hp}^+(z) = \frac{T_{hp}}{\Delta T_{max}}$$

50

Thus, the heat pipe convection Π group is about the balance between the maximum heat pipe convection heat transfer and maximum solid thermal energy:

$$\Pi_{hp,conv} = \frac{L[(\pi D)]\, h_{s,hp} \Delta T_{max}}{\dot{Q}_{s,max}}$$

51

By deriving the normalized axial position (z^+), the heat pipe energy residence time is given by the following:

$$z^+ = \frac{z}{L}$$

52

$$\tau = \frac{L(\rho_s C_s A_s \Delta T_{max})}{\dot{Q}_{s,max}}$$

53

The normalized time (t^+) is:

$$t^+ = \frac{t}{\tau}$$

54

When determining the conductive and convective Π groups, and heat pipe energy residence times, the remaining terms on the RHS develops a new Π group about the balance between the heat pipe stored heat and solid block stored heat:

$$\Pi_{hp/s,cap} = \frac{\rho_{hp} C_{hp} A_{hp}}{\rho_s C_s A_s}$$

55

Overall, the final normalized heat pipe energy balance equation is:

$$\Pi_{hp/s,cap}\frac{\partial {T_{hp}}^{+}}{\partial t^{+}} = \Pi_{hp,conv}\left({T_s}^{+} - {T_{hp}}^{+}\right) - \Pi_{hp,cond}\frac{\partial^2 {T_{hp}}^{+}}{\partial^2 z^{+}}$$

56

The LHS term represents the dimensionless energy change rate within the heat pipe. The first term on the RHS represents the dimensionless heat transfer rate from the block to the heat pipe, the second term the axial heat conduction along the heat pipe in the z-direction, the final term the heat removal rate from the heat pipe. Since the block surface is insulated shown in Figure 2.4, the radiative heat loss could be very small and therefore negligible.

The boundary condition on the insulated side of the heat pipe and its dimensionless form are given by:

$$\frac{\partial T_{hp}(z)}{\partial z} = 0$$

57

and

$$\frac{\partial {T_{hp}}^{+}}{\partial z^{+}} = 0$$

58

Recall, the boundary condition conductive heat transfer ($\dot{Q}_c$) was defined to be mid-way axial position in the heat pipe in Eq. 38. The boundary condition on the condenser side of the heat pipe and its dimensionless form are given by:

$$\dot{Q}_c = -kA_{hp}\frac{\partial T_{hp}(z)}{\partial z}$$

59

$$\dot{Q}_c^{+} = -\Pi_{hp,cond}\frac{\partial {T_{hp}}^{+}}{\partial z^{+}}$$

60

4.2. Lumped Approach

For this section, a period of time within the MAGNET experimental data were chosen after the rod heaters and gas heat removal system are turned off to determine heat losses. At roughly ~23,500 seconds the heat power falls to 0 and at ~25,500 seconds the gas mass flow rate falls to 0 indicating that heat generation and active heat removal have stopped. With these two conditions, characterizing the heat loss and heat transfer coefficient becomes somewhat simplified.

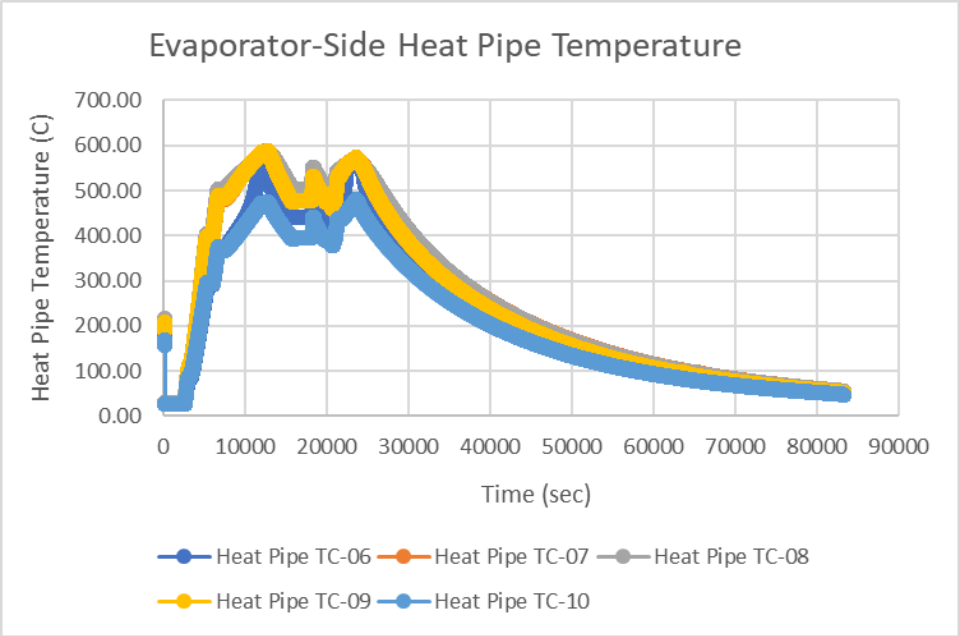

Figure 4.1 Evaporator-side thermocouple data. TC-10 is located deeper in the evaporator and TC-06 is near the transition to the condenser-side.

Heat pipe lumped approach:

$$\frac{L}{2}\left(\rho_{hp}C_{hp}A_{hp}\right)\frac{\partial \bar{T}_{hp,L/2}}{\partial t} = \left(\pi D_{hp}\frac{L}{2}\right)\bar{h}_{s,hp,L/2}\left(\bar{T}_{s,L/2} - \bar{T}_{hp,L/2}\right) - \dot{Q}_c \quad (61)$$

Where $\bar{T}_{hp,L/2}$ is the average heat pipe temperature mid-way axial, $\bar{h}_{s,hp,L/2}$ is the average convective heat transfer coefficient mid-way axial, and $\bar{T}_{s,L/2}$ is the average solid temperature mid-way axial. In this decay period with the rod heaters, the gas cooling is off:

$$\dot{Q}_c \approx k_{sodium}\frac{T_{hp,6} - T_{hp,5}}{L_{6,5}}A_{hp} \quad (62)$$

Where $T_{hp,6}$ is the heat pipe temperature at TC-06, $T_{hp,5}$ is the heat pipe temperature at TC-05, and $L_{6,5}$ is the spacing between TC-06 and TC-05. For treatment of the axial heat conduction term, a temperature dependent thermal conductivity, k_{sodium}, was used across the operating range to improve accuracy, although it is mostly linear.

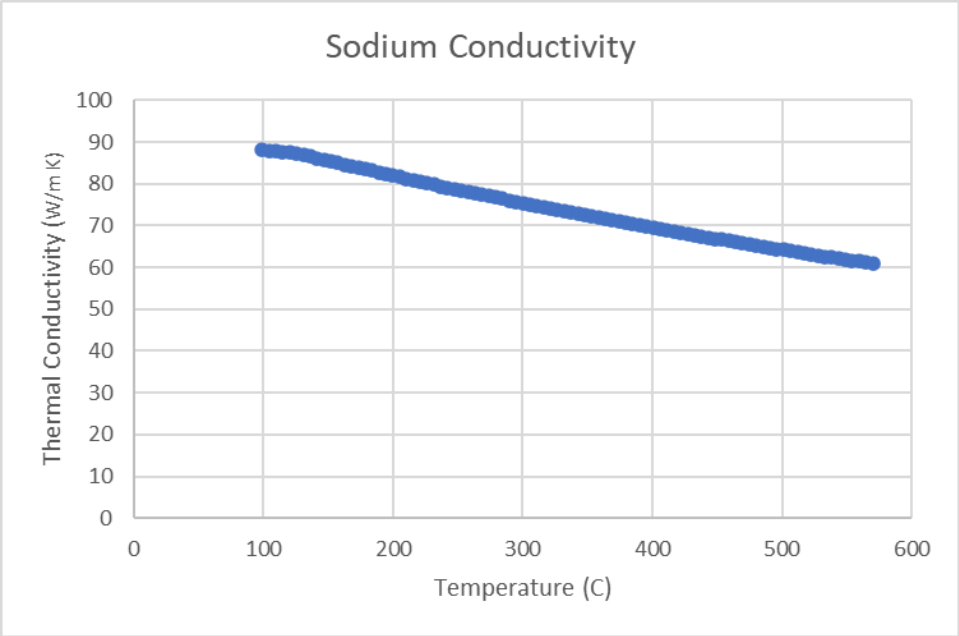

Figure 4.2 The sodium conductive heat transfer coefficient based on the average temperature at mid-way axial position.

By separating the heat transfer term from the block to the heat pipe and plugging into the block equation, an alternate form of the lumped approach can be derived:

$$\frac{L}{2}\left(\rho_{hp}C_{hp}A_{hp}\right)\frac{\partial \bar{T}_{hp,L/2}}{\partial t} = \left(\pi \mathrm{D}_{hp}\frac{L}{2}\right)\bar{h}_{s,hp_{L/2}}\left(\bar{T}_{s,L/2} - \bar{T}_{hp,L/2}\right) - \dot{Q}_c$$

63

$$\left(\pi \mathrm{D}_{hp}\frac{L}{2}\right)\bar{h}_{s,hp_{L/2}}\left(\bar{T}_{s,L/2} - \bar{T}_{hp,L/2}\right) = \frac{L}{2}\left(\rho_{hp}C_{hp}A_{hp}\right)\frac{\partial \bar{T}_{hp,L/2}}{\partial t} + \dot{Q}_c$$

64

Move the heat loss term to the LHS:

$$\dot{Q}_c + \frac{L}{2}\left(\rho_{hp}C_{hp}A_{hp}\right)\frac{\partial \bar{T}_{hp,\frac{L}{2}}}{\partial t} = \left(\pi \mathrm{D}_{hp}\frac{L}{2}\right)\bar{h}_{s,hp_{\frac{L}{2}}}\left(\bar{T}_{s,\frac{L}{2}} - \bar{T}_{hp,\frac{L}{2}}\right)$$

65

By rearranging Eq. 65 to solve for the heat loss term, the boundary conductive heat transfer is:

$$\dot{Q}_c = \left(\pi \mathrm{D}_{hp}\frac{L}{2}\right)\bar{h}_{s,hp_{L/2}}\left(\bar{T}_{s,L/2} - \bar{T}_{hp,L/2}\right) - \frac{L}{2}\left(\rho_{hp}C_{hp}A_{hp}\right)\frac{\partial \bar{T}_{hp,L/2}}{\partial t}$$

66

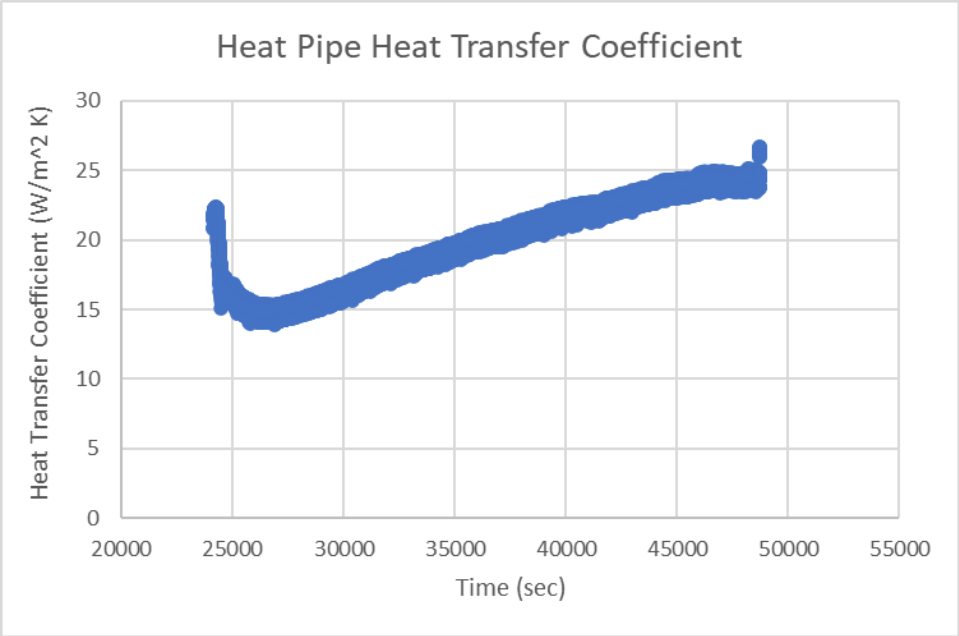

Figure 4.3 Transient heat pipe heat transfer coefficient based on the lumped approach when the boundary conducted heat transfer is calculated via the provided equations and transient temperature data in Figure 2.5.

As shown in Figure 4.3, the heat transfer coefficient is within a reasonable value in the chosen range, however there is a small section toward the beginning showing the difference in heat removal and heat addition as the heater rods and gas cooling were turned off at slightly different times.
To compare the heat transfer coefficient found using the lumped approach in a decay-heat like state at the previously described conditions, we select a period of relative steady-state behavior. This state takes place at roughly 16,200–18,000 seconds where the gas mass flow rate and heater power are mostly constant. We calculate a much more constant heat transfer coefficient, shown in Figure 4.4, that is within reasonable proximity to the transient heat transfer coefficient shown in Figure 4.3.

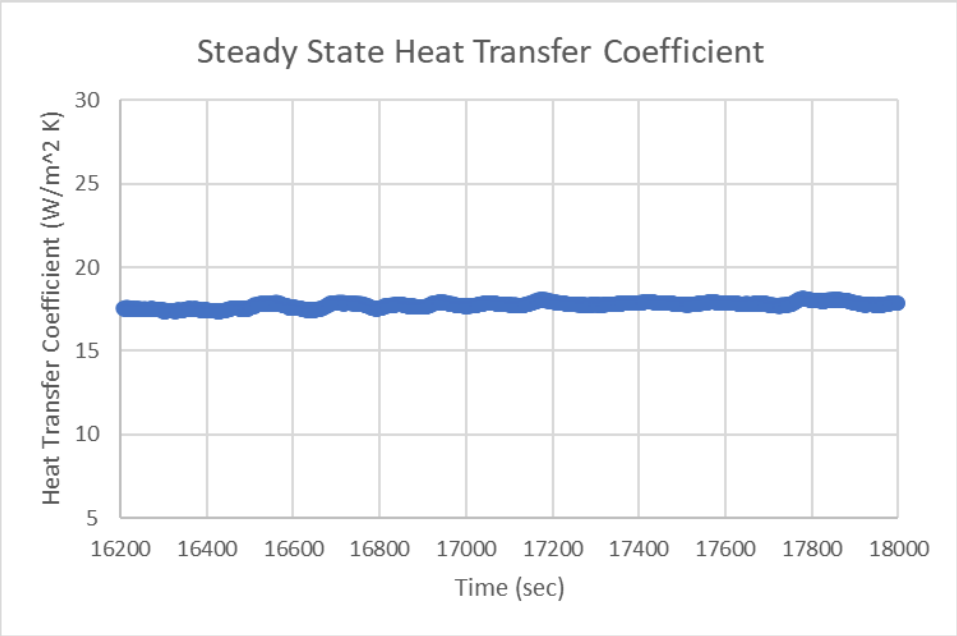

Figure 4.4 Steady-state heat transfer coefficient based on the lumped approach when the boundary conducted heat transfer is calculated via the provided equations and pseudo-steady temperature data in Figure 2.5.

5. FUTURE WORK

The next steps include scaling using Dynamical System Scaling (DSS) methodology to further analyze and characterize the transient response of the system. As the intended purpose of scaling MAGNET was to connect it to the other scaled facilities, Thermal Energy Distribution System (TEDS) and High Temperature Steam Electrolysis (HTSE), within DETAIL. There is still some work left to be completed regarding connecting those with DSS. As is standard with DSS, there is data processing that still needs to be completed along the way to determine validity and conducting diagnostic steps.

6. CONCLUSION

Several scenarios were chosen to analyze and develop first principles equations for the MAGNET system. Since this effort had the benefit of experimental data to diagnose and correct assumptions made developing the governing equations, there were opportunities to separate sections of the data and extract important characteristics. One being the heat transfer coefficient, which can be challenging to determine due to the dependence on multiple factors such as flow behavior, geometry, power levels, etc. The heat transfer coefficient was required for the overall heat removal behavior since there were periods of heating, active cooling, and passive cooling. With the developed governing equations and axial conduction term using a temperature dependent thermal conductivity for sodium within the heat pipe, the system was able to be characterized and analyzed. Further, the scaled equations using H2TS were made with some operational characteristics in mind.

Since this system and the experimental data include interesting transient behavior, there is still work in progress towards using DSS to further connect MAGNET to the other facilities such as TEDS or HTSE. Although H2TS and DSS are distinct scaling methodologies, they root from the same concept of utilizing governing and process equations to derive normalized expressions that help scale the system of interest. The work developed in this report can be applied to the DSS analysis with minimal effort and will support

the future activities to make the conversion. One essential aspect of the current analysis is that it provides the scaling framework for steady-state operations. The majority of the operational conditions for the target nuclear reactors and the intended industrial processes to couple are for normal operations without transient behavior. The analysis provided in this report exactly provides the framework to design meaningful experiments and scale-up installations during normal operations. After applying the equations to DSS and testing the dynamic behavior during transients (e.g., startup, shutdown, or any operation deviating from normal operations), the necessary adjustments can be made towards the determined experiments and facility design.

7. REFERENCES

1. Sabharwall, P., Hartvigsen, J. L., Morton, T. J., Yoo, J., Qin, S., Song, M., Guillen, D. P., Unruh, T., Hansel, J. E., Jackson, J., Gehin, J., Trellue, H., Mascarenas, D., Reid, R. S., and Petrie, C. M. 2023. Nonnuclear Experimental Capabilities to Support Design, Development, and Demonstration of Microreactors, Nuclear Technology, 209:sup1, S41-S59. DOI: https://doi.org/10.1080/00295450.2022.2043087.
2. Martin, R. P., and Frepoli C., eds. 2019. Modern Nuclear Energy Analysis Methods: Design-Basis Accident Analysis Methods for Light-Water Nuclear Power Plants.3: 181–263. Singapore: World Scientific. DOI: https://doi.org/10.1142/11139.